Parasitology Research (2019) 118:1609–1623
https://doi.org/10.1007/s00436-019-06286-x

PROTOZOOLOGY - ORIGINAL PAPER

Detection and characterization of an albumin-like protein in *Leishmania donovani*

Bhakti Laha[1] · Amit Kumar Verma[1] · Bapi Biswas[1] · Satheesh Kumar Sengodan[1] · Akanksha Rastogi[1] · Belinda Willard[2] · Monidipa Ghosh[1]

Received: 3 September 2018 / Accepted: 4 March 2019 / Published online: 22 March 2019

Abstract

The protozoan parasite, *Leishmania donovani*, undergoes several molecular adaptations and secretes many effector molecules for host cell manipulation and successful parasitism. The current study identifies an albumin-like secretory protein, expressed in its extracellular promastigote forms. A leishmanial complementary DNA sequence of a partial gene has been cloned, and the encoded peptide (14 kD) is used for the production of polyclonal antibody. This targeted antibody identifies a large native protein (66.421 kD), expressed stage-specifically in promastigotes. Through electron microscopic studies, the native protein is found to be localized in the flagellar pocket and flagella and at the surface of the promastigotes. This native protein is purified with the same customized antibody for future characterization and sequencing. The sequence analysis reveals its homology with the mammalian serum albumin. It is evidenced from in silico studies that this albumin-like protein remains associated with long-chain fatty acids while in vitro studies indicate its close association with membrane cholesterol. Since antibody-mediated blocking compromises the parasite infectivity, these leishmanial albumin-like molecules are hereby proposed to play an instrumental role in the infectivity of *L. donovani* to peripheral blood monocyte cells. Thus, identification and characterization of an albumin-like protein in *L. donovani* promastigotes may be interpreted as a molecular adaptation candidate. It may be hypothesized that the parasite mimics the mammalian system for importing fatty acids into the intracellular amastigotes, facilitating its host cell infectivity.

Keywords Visceral leishmaniasis · Promastigote-specific · Albumin-like protein · Flagella · Flagellar pocket · Cholesterol colocalization · PBMC infection

Introduction

Leishmaniasis is a broad-spectrum parasitic disease affecting different types of tissues in mammals (Piscopo and Mallia Azzopardi 2007). The causative agents of the disease are the different species of *Leishmania* that choose the skin, mucous membrane, and visceral organs of the body for their colocalization according to the etiology of the infecting species (Farrell 2002). Visceral leishmaniasis that is caused by the parasites *Leishmania donovani* and *Leishmania infantum* is fatal (McCall et al. 2013). This trypanosomatid parasite exists in two different life forms: flagellated promastigotes and aflagellated amastigotes (Sunter and Gull 2017).

Parasites take part in active immune modulation to get control over their host system, for their successful parasitism (Gupta et al. 2013). *Leishmania* is known to adapt several host cell–evading machineries among which lipophosphoglycan, GP63, directly interacts with the host cell membrane (Lodge et al. 2006; Atayde et al. 2016; Soulat and Bogdan 2017), whereas EF1α, fructose-1,6-biphosphate aldolase, and SAcp get access into host cells by directly crossing either the plasma membrane or through the membrane of parasitophorous

Section Editor: Sarah Hendrickx

Electronic supplementary material The online version of this article (https://doi.org/10.1007/s00436-019-06286-x) contains supplementary material, which is available to authorized users.

✉ Monidipa Ghosh
gmonidipanitd@gmail.com

[1] Department of Biotechnology, National Institute of Technology Durgapur, Mahatma Gandhi Avenue, Durgapur, West Bengal 713209, India

[2] Mass Spectrometry Laboratory for Protein Sequencing, Cleveland Clinic - Lerner Research Institute, 9500 Euclid Avenue, Cleveland, OH 44195, USA

vacuole where amastigotes reside and grow (Nandan et al. 2002; Fernandes et al. 2013; Gupta et al. 2014).

Leishmania and other trypanosomatids evade the host cell immune response by different MAP kinase pathways (Soares-Silva et al. 2016) and the phosphatases (Shio et al. 2012). It is reported that PI3-AKt kinase and phosphatidylinositol 3-phosphate (PI3P) are involved in the host cell immune evasion in BALB/c $p^{85-/-}$ mice model (Ruhland et al. 2007; Kima 2016). In *Leishmania*, the metabolism of sphingolipids (SLSs) like ceramides has gained considerable attention because of their biological relevance in parasite infectivity and disease progression (Pillai et al. 2012). Ceramide with palmitate (C16) and stearate (C18) as their long-chain fatty acids (Hsu et al. 2007; De Castro Levatti et al. 2017) is conjugated with phosphatidylinositol to form inositol phosphorylceramide (IPC) (Hsu et al. 2007; Mina et al. 2011) and is considered as a potentially useful target chemotherapy against leishmaniasis. This unusually long fatty acid chain in IPC of *Leishmania* indicates the use of myristoyl CoA for ceramide synthesis (Zhang and Beverley 2010). Comparative analysis of fatty acids in both promastigotes and amastigotes exhibits selective upregulation in the amounts of palmitate being abundant in the triacylglycerol (Bouazizi-Ben Messaoud et al. 2017).

In our laboratory, 57 species-specific genes of *L. donovani* have been identified, among which 38 genes are assigned with putative function through in silico studies. One partial gene, annotated as AMA1 (Gene ID: LBPK_301490), has been studied for its expression and putative role in *L. donovani* parasitism which is being reported here (Sengodan et al. 2014). The purified native protein is found to share a high sequence similarity with albumin and colocalizes with membrane cholesterol molecules, interacting with the palmitate and myristate as putative ligands. The study supports that *Leishmania* requires a greater amount of palmitate and myristate for the synthesis of PI3P, IPC as sphingolipids, phospholipids, and triacylglycerol, which helps in successful parasitism.

Methods

Cell and parasite culture

L. donovani (AG83) promastigotes were maintained at 22 °C in M199 media supplemented with 10% FCS, penicillin (50 U/ml), and streptomycin (50 μg/ml) (Gibco). Promastigotes were harvested in late log phase (10 million promastigotes/ml) by centrifugation at 1200*g* for 10 min and washed with phosphate buffer (PB) (pH 7) (Roychoudhury and Ali 2008). Human cell line THP1 was maintained in RPMI (Gibco) media similarly supplemented with FCS, penicillin, and streptomycin (Das et al. 2001). The promastigotes were transformed into amastigotes by infecting THP1 cells with *L. donovani* promastigotes at a ratio of 1:5 (cell:parasite). Finally, the amastigotes were isolated following the method described with some modifications (Lúcia et al. 1998).

Cloning of the partial gene ama1

The partial gene (Gene ID: LDBPK_301490) was PCR amplified from the purified genomic DNA of *L. donovani* promastigotes (Beck 2002), and the fragment was incorporated into the pET20b(+) vector at its multiple cloning site using the restriction sites of *Bam*HI and *Hin*dIII. The pET-ama1 construct was used to transform the *Escherichia coli* DH5α and BL21 strains for maintenance and expression hosts, respectively. For the details of cloning and primers, the Additional Information, Additional File, may be referred.

Confirmation of cloning through colony PCR, plasmid DNA sequencing, and Western blotting

Colony PCR with transformed and untransformed DH5α and BL21 cells was done using the same Ama1-F and Ama1-R primers and same PCR program, adding a single colony from the transformed and untransformed DH5α plate instead of the template DNA. Plasmid isolation was done with plasmid purification mini kit (Qiagen) from transformed DH5α cells. Single-strand sequencing was performed with the isolated plasmid dissolved in 20 μl of DEPC-treated water by Xcelris Labs (Bengaluru, India). The chromatogram was uploaded in the National Center for Biotechnology Information (NCBI) for BLASTn, for checking the identity with the available partial sequence in the database. To observe the expression of AMA1 in the transformed *E. coli* BL21 cells with respect to other control (for details, go to the Additional Information, Additional File), the bacterial pellets were dissolved in ~500 μl of cell lysis buffer (20 mM Na_2HPO_4, 300 mM NaCl, pH 8.5) in the presence of lysozyme (Sigma), PMSF (Sigma), and bacterial protease inhibitor (Amresco) at 4 °C followed by Western blot analysis. The recombinant partial protein with the C-terminal 6× histidine tag was probed with the anti-6× His tag antibody and anti-mouse HRP secondary antibody at indicated dilutions on PVDF membrane.

Purification of the partial protein

IPTG concentration was optimized at 0.5 mM for induction to avoid entrapment of the target protein into inclusion bodies. The partial recombinant AMA1 with a C-terminal 6× His tag was purified with the Ni beads (Thermo Scientific 88221) in eight fractions (E1–E8) according to the protocol described in the Additional Information, Additional File (Spriestersbach et al. 2015). The eluted fractions (E5–E8) were collectively

dialyzed and lyophilized at vacuum, at a temperature of − 50 °C for 24 h. The different purified fractions were checked for the presence of the partial protein and quantified with the Bradford assay.

MALDI-TOF MS and LC-MS analysis

The lyophilized dialysates of the partial protein and the purified native protein were observed in MALDI-TOF MS to detect its purity and post-translational modifications. The dissolved protein was spotted on a target MALDI plate using α-cyano-hydroxycinnamic acid (CHCA) as a matrix and analyzed using a MALDI-TOF mass spectrometer (Applied Biosystems, USA). Spectra were calibrated using the matrix. These studies were done in CSIR-IICB Kolkata using the central instrumentation facility for mass spectrometry (MALDI) (Raghwan and Chowdhury 2014). LC-MS analysis of the native protein was performed after the trypsin digestion of the SDS-PAGE–entrapped peptide.

Production of customized antibody and ELISA

The production of customized antisera against the purified partial protein was outsourced from Abgenex Pvt., Ltd. (Bhubaneswar, India). A rabbit model was immunized with a solution containing the partial protein in 0.9% saline. The serum was collected from the animal before (prebleed) and after 1 month of the first booster dose injection (first bleed) and 15 days after the second and third booster doses (second bleed and third bleed) (Buffer et al. 2013). Indirect ELISA was done twice. The first ELISA was done with 200 ng of purified AMA1 protein and all the collected rabbit sera (prebleed, first bleed, second bleed, and third bleed) (1:5000) while the second experiment of ELISA was with promastigote lysate in order to detect the level of expression. The lysate and the antisera (prebleed and third bleed) were used in dilutions of 1:100 and 1:1000, respectively. In both ELISA experiments, anti-rabbit HRP secondary antibody (BD554021) (1:5000) and 3,3′,5,5′-tetramethylbenzidine (TMB)-H_2O_2 solution (Sigma) were used for detection of the titer with 0.1 mM acidic atop solution (λ = 450 nm) (Cox et al. 2004).

Fluorescence microscopy

The localization of the native protein and its colocalization with 22-(N-(7-Nitrobenz-2-Oxa-1,3-Diazol-4-yl)Amino)-23,24-Bisnor-5-Cholen-3β-Ol (NBD)-labeled cholesterol of all the *L. donovani* promastigotes and *L. donovani*–infected THP1 cells were performed using fluorescence microscopy. The target native protein was stained with the raised third bleed antiserum and anti-rabbit rhodamine secondary antibody (Das et al. 2001). The NBD-labeled cholesterol produces green fluorescence, visible at 591 nm. All the observations were done under a fluorescence microscope (Zeiss) at 63× magnification and oil immersion after mounting with media containing DAPI. Similar optical filters were used for DAPI (λ = 461 nm), FITC (λ = 591 nm), and PI (λ = 636 nm) for the parasites and infected cells stained with the prebleed serum as negative controls.

Immune electron microscopy

The *L. donovani* promastigotes were checked for the native protein in the subcellular compartments using TEM (Tecnai TEM; SAIF AIIMS, New Delhi) after probing with the prebleed and third bleed fractions of the customized antisera and protein A–nanogold particles. The other subcellular structures were stained with 1% aqueous uranyl acetate and alkaline lead citrate (Escalona-Montaño et al. 2017). (For details, go to the Additional Information, Additional File).

Two-step reverse transcription PCR

The presence of AMA1 in the transcript level of both forms of the promastigotes and amastigotes of *L. donovani* was checked by isolating whole-cell RNA from *L. donovani* promastigotes and amastigotes with TRI Reagent (Sigma T9424). Then, the reverse transcriptase enzyme was used for complementary DNA (cDNA) preparation at 37 °C for 20 min from the whole-cell messenger RNA (mRNA) with the same AMA1-F and AMA1-R primers. In the next step, PCR was done with the program set with a T_m value of 69.5 °C and by adding 5 μl of the cDNA (Couvreur et al. 2003).

Purification of the native protein, using the oriented affinity method of immunoprecipitation assay

The third bleed serum was used for purification of native protein following the principles of the oriented affinity method of immunoprecipitation (Kowal and Parsons 1980) (discussed in the Additional Information, Additional File).

Pairwise sequence alignment

The LC-MS analysis led us to an amino acid sequence which was uploaded to the tools of EMBOSS (https://www.ebi.ac.uk/Tools/psa/), i.e., Needle, Stretcher, and Matcher, and the partial sequence from the database was examined for pairwise sequence alignment with the full amino acid sequence obtained after LC-MS analysis. The EBLOSSUM62 matrix was used for the local alignment of two sequences (Rice et al. 2000; McWilliam et al. 2013; Li et al. 2015).

Alignment and 3D structure prediction with the SWISS-MODEL system and COACH server

The amino acid sequence obtained after LC-MS analysis was first subjected to BLASTp and conserved domain search in the NCBI site. Satisfactory similarity with serum albumin (UniProtKB AC: P02768) took us for 3D structure predictions (Marchler-Bauer et al. 2017). The structure prediction was done through both approaches of homology modeling and protein threading. The sequence was uploaded to both the SWISS-MODEL system (https://SWISSmodel.expasy.org/interactive) (Arnold et al. 2006; Kiefer et al. 2009; Guex et al. 2009; Biasini et al. 2014) and COACH server (Yang et al. 2013a, b) (https://zhanglab.ccmb.med.umich.edu/COACH/). In the SWISS-MODEL system, 1bj5.1.A (human serum albumin complexed with myristate) and 4bke.1.A (recombinant human serum albumin complexed with palmitate) were used as templates for the 2× myristic acid (MYR)-bound and 2× palmitic acid (PLM)-bound models of the native protein, whereas in the COACH server, the structure was predicted by MUSTER with the template 1n5ua (X-ray study of human serum albumin complexed with heme) (z score = 23.675, cutoff = 6.1). For structure validations, the .pdb files of the predicted models were obtained checked with the following compiled tools: ERRAT (Colovos and Yeates 1993), PROVE (Pontius et al. 1996), and Ramachandran plot and VERIFY_3D (Bowie et al. 1991; Lüthy et al. 1992) of SAVES (https://services.mbi.ucla.edu/SAVES/) as well as the ProSA tools (Wiederstein and Sippl 2007) (https://prosa.services.came.sbg.ac.at/prosa.php). The z score of the model predicted from the COACH server was produced in the site. Finally, the qualities of all the three models binding to their putative ligands were checked using PROCHECK (http://services.mbi.ucla.edu/PROCHECK/) (Morris et al. 1992; Laskowski et al. 1993; Furey et al. 2006).

Cholesterol colocalization assay

The colocalization assay of the leishmanial native protein with cholesterol in both promastigotes and infected cells was done by labeling the promastigotes and mammalian THP1 cells with green fluorescent NBD-labeled cholesterol (591 nm) (Brasselet et al. 2013). The leishmanial native protein was then stained with its third bleed sera and anti-rabbit rhodamine secondary antibody for tracing colocalization through fluorescence microscopy, using the respective filters (Additional Information, Additional File).

Peripheral blood mononuclear cell infection assay

The role of native protein in infection was established by using the peripheral blood mononuclear cell (PBMC) collected from freshly drawn blood (Verma et al. 2017). The isolated PBMCs were plated in lysine-coated culture plates and infected with *L. donovani* promastigotes that were provided in 1:5 ratios (Inf). For this experiment, three groups were designed. Uninfected PBMCs were used as negative control (Uninf). The *L. donovani* promastigotes preincubated with the third bleed serum were considered as the treated–infected group (T-Inf). The incubation was done at 22 °C for 1 h which blocked the albumin-like molecules present on the surfaces of the parasite with the polyclonal antibody in the third bleed serum. After incubation, the promastigotes were thoroughly washed with phosphate buffer and then used for infection. The infectivity was observed for 3 days at an interval of 24 h and expressed in percent infection.

Accession numbers

The IDs and annotations for the partial protein sequence are as follows: EnsemblProtists[i] (CBZ36170; CBZ36170; LDBPK_301490), GeneDB[i] (LdBPK_301490.1.1:pep), GeneID[i] (13385569), and KEGG[i] (ldo:LDBPK_301490).

Results

Overexpression of the leishmanial partial gene (LDBPK_301490) and confirmation

The only available gene sequence from the database is partial for our target gene ama1. To characterize the full-length native protein in *L. donovani*, polyclonal antibody was raised against this partial peptide. The 246-bp-long partial gene sequence was cloned in-frame in the pET20b(+) expression vector with its own start codon with a C-terminal 6× His tag, under the Tac promoter, and was amplified in *E. coli* DH5α cells (Fig. S1.a.L4). The amplified plasmid construct (pET-ama1) was isolated from these transformed DH5α cells and was used for nucleotide sequencing.

The chromatogram (Fig. S1.b) confirmed the desired attempt of cloning with 99% similarity (Fig. S2) in respect to *L. donovani* ama1 (LDBPK_301490) mRNA when uploaded in the NCBI for BLASTn. This confirmation led us to transform the expression host, *E. coli* BL21 cells, for expressing the partial peptide AMA1. It was further confirmed through colony PCR (Fig. S1.a.L2) and used for bulk production of the partial protein for purification.

Expression and purification of the leishmanial partial peptide for immunization

Expressions of the leishmanial partial peptide

The transformed BL21 cells were then induced for overexpression of the partial peptide. The presence of a protein band

of ~ 14 kD was compared in the crude lysates of the induced cells with the cells with the empty pET20b(+) vector when probed with the anti-His antibody after Western blot analysis (Fig. S1.c.L5). This confirmed the expression of the targeted leishmanial partial peptide in the prokaryotic environment.

In order to raise the customized antibody, ~ 5 mg of the partial peptide was necessary for immunizing a rabbit. The transformed bacterial cells were induced to produce the 14 kD partial protein with a carboxy-terminal histidine tag. This histidine tag was used to purify the partial peptide from the crude bacterial extract with Ni beads ("Methods"). The elutes (four to seven) (Fig. S1.d.L1 and L3 to L5) and the dialysate (Fig. S1.d.L6) all contained the recombinant partial protein (14 kD) without any other peptide contaminant while the rest of the fractions were sequestered through repeated reloading and elution with Ni beads. Approximately 5 mg of the partial peptide was purified from 1 l of broth (Fig. 1a). After dialysis, the molecular weight and purity of the partial protein were determined by MALDI-TOF MS analysis of the lyophilized sample. The *m* peak at 14,296.7 D in MALDI-TOF MS indicated the molecular weight of the purified partial peptide, and the *m*/2 peak at 7143.4 D (Fig. 1b) indicated the expressed leishmanial partial peptide to be without any post-translational modification in a prokaryotic system.

Production of antiserum against the partial peptide

The purified partial peptide was used for immunizing a rabbit. The serum collected before and after the first, second, and third immunizations was labeled as prebleed, first bleed, second bleed, and third bleed sera, respectively. These sera were tested for the titer of polyclonal antibody against the leishmanial partial peptide through indirect ELISA. Among all the varieties of antisera, the third bleed serum contained the highest titer of polyclonal anti-AMA1 antibody (Fig. 1c) and used for further characterization assays, viz. immune localization and immunoprecipitation.

Immune localization of the native protein in *Leishmania donovani*

Localization of the native protein in the promastigotes by fluorescence microscopy

Fluorescence microscopy with the fixed *L. donovani* promastigotes, probed with the third bleed antiserum, revealed the presence of the native protein at both the cytoplasm and flagella. Although the exact localization within the promastigote cytoplasm was not very clear, the flagella took a very precised fluorescent stain (Fig. 2a), indicating the native protein to be a flagellar one, in respect to the negative control stained with the prebleed sera (Fig. 2b).

Subcellular localization of the native protein in the promastigotes by immune electron microscopy

To investigate the exact location of the native peptide in the *L. donovani* promastigotes, immune electron microscopy (IEM) was attempted. The IEM results indicated the native peptide to be mainly present in the flagellar pocket and at the base of the flagella. The flagellar structure exhibited an intermittent electron dense region as the site of the target native protein (Fig. 2c, panel III). Cytoplasmic vesicles as well as surfaces also exhibited the presence of the target protein (Fig. 2c, panel II). A comparative index of subcellular localization has been displayed for a clear understanding in Table 1.

The average subcellular distribution of the nanogold dots clearly indicates the native peptide to be mostly available in the flagellar pocket and flagella and at the cell surface protein. The subcellular distribution of the native protein indicates that it may have its way through the flagellar pocket which is a well-established vestibule in the *Trypanosomatids*.

Stage-specific expression and characterization of the native protein in *L. donovani* promastigotes

The selective abundance of the native protein in the flagella and flagellar pocket and at the cell surface region led us to investigate its expression and presence in the amastigotes of *L. donovani*. The cDNA of both the forms of *L. donovani* was obtained through reverse transcription with the whole-cell RNA extracted. PCR with the primers specified for the partial gene gave a clear band near 250 bp (Fig. 3a, L2) for the promastigotes whereas bands of non-specific amplifications were obtained for the amastigotes (Fig. 3a, L3). This proved that the mRNA for the expression of the known partial part of the native protein was absent in the amastigotes while promastigotes were found to have abundant mRNA for the expression of the native protein.

After proper fixation, both the stages of *L. donovani* were also checked for the presence of the native protein through fluorescence microscopy. But, the protein is found to be present in both the promastigotes (Fig. 3b, panel i) and the infected cells (Fig. 3b, panel ii). The presence of this native protein in the infected cells in contrast to the RT-PCR results with the amastigotes indicates its potential role in infection and parasitism.

Characterization of the native protein from *L. donovani* promastigotes

Purification and full sequencing of the native protein

Complete characterization of the native protein detected in the promastigotes required its purification from the crude parasitic

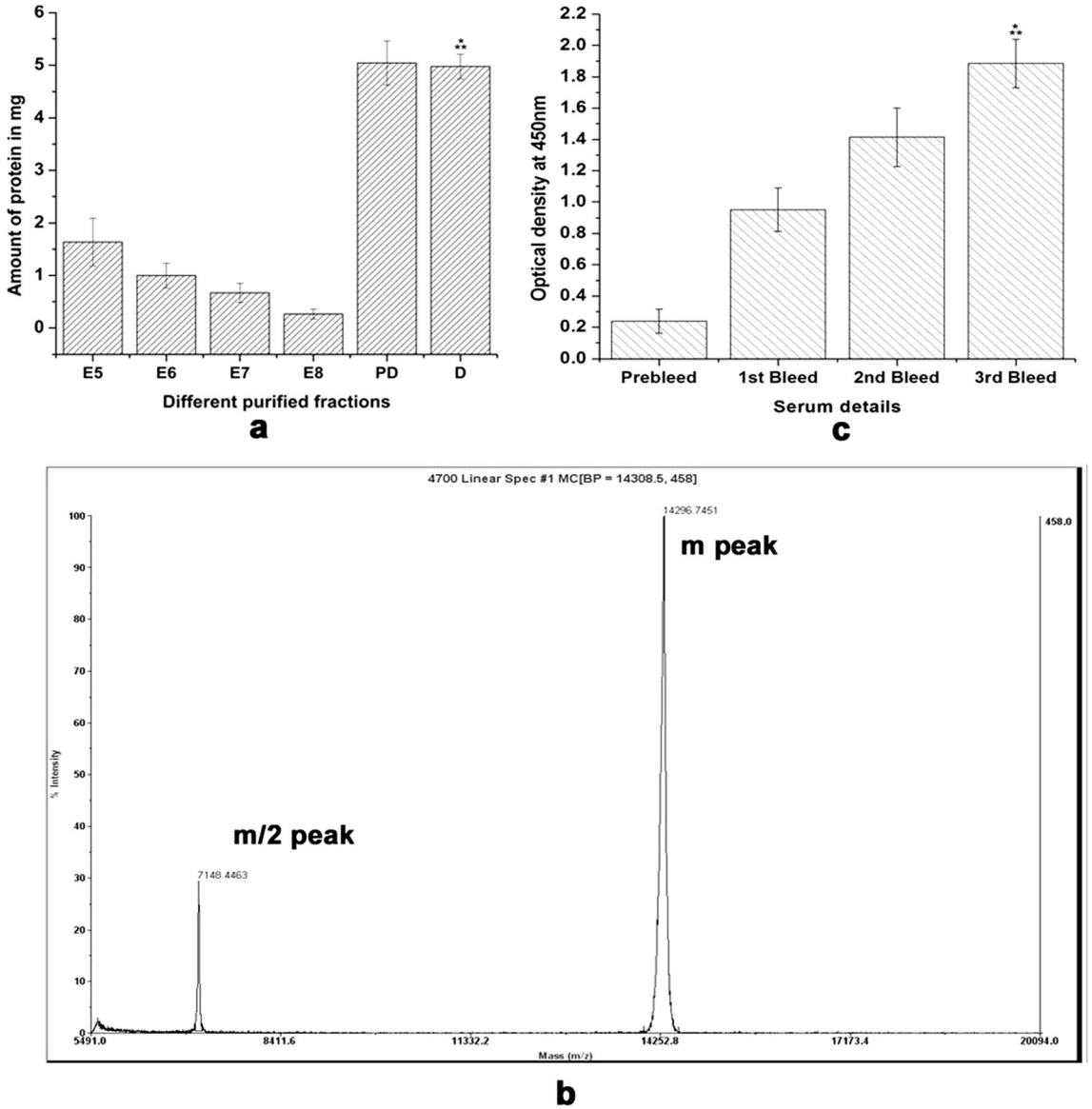

Fig. 1 Quantitative and qualitative estimations of the purified partial protein and the polyclonal antisera raised against it. **a** Quantification of the partial peptide in different fractions and dialysates after its purification with Ni bead. E5–E8: amount of the partial protein in the elutes, collected after washing the Ni beads with elution buffer containing 100 mM of imidazole at the fifth to eighth times; PD: amount of the partial protein in the solution with all the collected purified elutes before dialysis; D: amount of the partial protein in the dialysate with all the purified elutes after dialyzing out the imidazole. **b** Qualitative estimation of the purified partial peptide with MALDI-TOF MS. *m* peak denotes the molecular mass of the purified partial peptide after being singly charged with laser. *m*/2 peak denotes the molecular mass of the same peptide when doubly charged with laser. **c** Checking of the polyclonal antibody in the different fractions of antisera, collected before and after the immunization process from the immunized rabbit, with indirect ELISA. Prebleed: serum collected from the rabbit before immunization; first bleed: serum collected after 1 month of the first booster dose; second and third bleed: serum collected after 15 days of the second and third booster doses, respectively

extract. Before purification, the level of expression of the native protein was checked through indirect ELISA assay with the third bleed serum. The expression was found to be adequate for purification and further characterization (Fig. 4a). The third bleed serum with the maximum amount of antibody against the partial peptide was used for purification of the native protein from the promastigote lysate. The polyclonal antibody molecules in both the third bleed and prebleed sera were cross-linked with protein A on Sepharose bead so that the heavy and light chains of the antibody do not come out with the bound antigen, viz. our target native protein, while being eluted. The purification was checked in the presence of other two negative controls: L3B and PPB. In L3B, the lysis buffer used in promastigote lysate was loaded in the bead column with protein A–third bleed serum (Fig. 4b, L2), and in PPB, the promastigote lysate was loaded in the protein A–

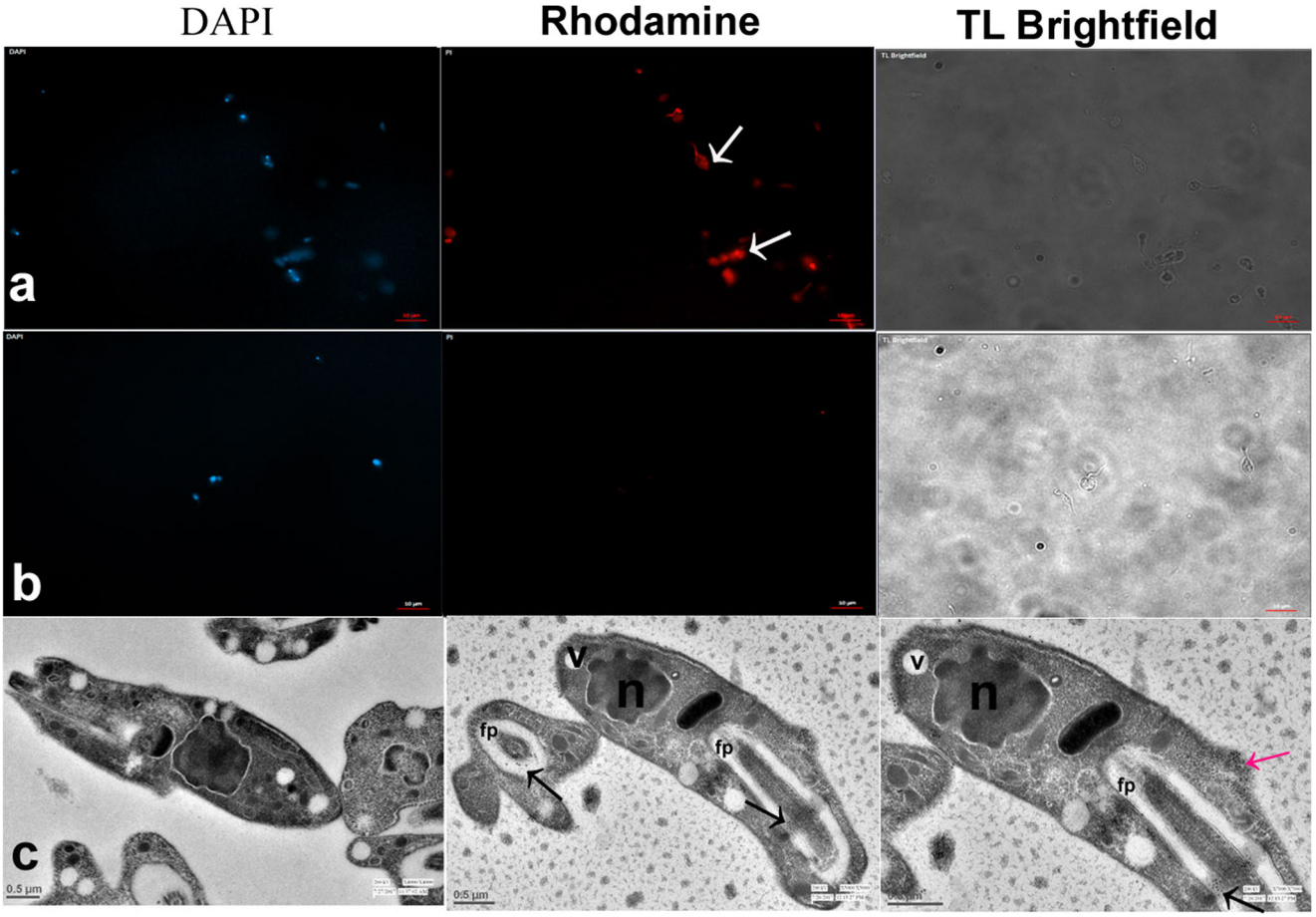

Fig. 2 Localization of the native protein in the promastigotes of *L. donovani* through fluorescence microscopy and immune electron microscopy. **a** Probing of the native protein with the third bleed antiserum and anti-rabbit rhodamine secondary antibody using the filters at 461 nm (DAPI) and 636 nm (rhodamine) and by phase contrast microscopy. **b** Promastigote native protein probed with the prebleed antiserum and the same secondary antibody acting as negative control. **c** TEM images of *L. donovani* promastigotes after immunostaining the native protein with the prebleed (negative control) and third bleed antisera, counterprobed with protein A–nanogold particles. Different annotations refer to different subcellular compartments. fp flagellar pocket, f flagella, s surfaces, v vesicles, n nucleus

prebleed column (Fig. 4b, L3). The absence of any band in any of these two control groups over-ruled any chances of contamination. But, the promastigote lysate produced a larger protein band near 71 kD (Fig. 4b, L4) after its incubation with the protein A–Sepharose bead cross-linked to the third bleed serum. This purified protein yielded its accurate molecular weight of 66.421 kD at MALDI-TOF MS analysis (Fig. 4c, peak M). In MALDI-TOF MS analysis data, an *m*/2 peak is also obtained at 33.349 kD which indicates the target protein, in its native form, may be devoid of any post-translational modification (Fig. 4c, peak *m*/2). To achieve its complete characterization, the full amino acid sequence was necessary which was obtained through LC-MS analysis (Fig. S3) with the pulled-down native protein. The CID spectra, when searched in the full NCBI database with the MS-Batch program, ended up with an amino acid sequence, with a SEQUEST score of 721.8 and a sequence coverage of 82.9 with serum albumin (Accession no. P02769).

Table 1 Comparative analysis of the subcellular localization of the native protein

Subcellular structures	Numbers of nanogold dots	Number of samples analyzed	Distribution of nanogold dots/cell
Flagella (f)	448	35	> 12
Flagellar pocket (fp)	467	39	> 11
Cell surface (s)	763	68	> 11
Nucleus (n)	169	24	> 7
Vesicles (v)	108	34	> 3

Alignment and 3D structure prediction from the sequence of the native protein

The search for conserved domain and pBLAST alignment was done using the NCBI tools (Fig. S5). pBLAST results

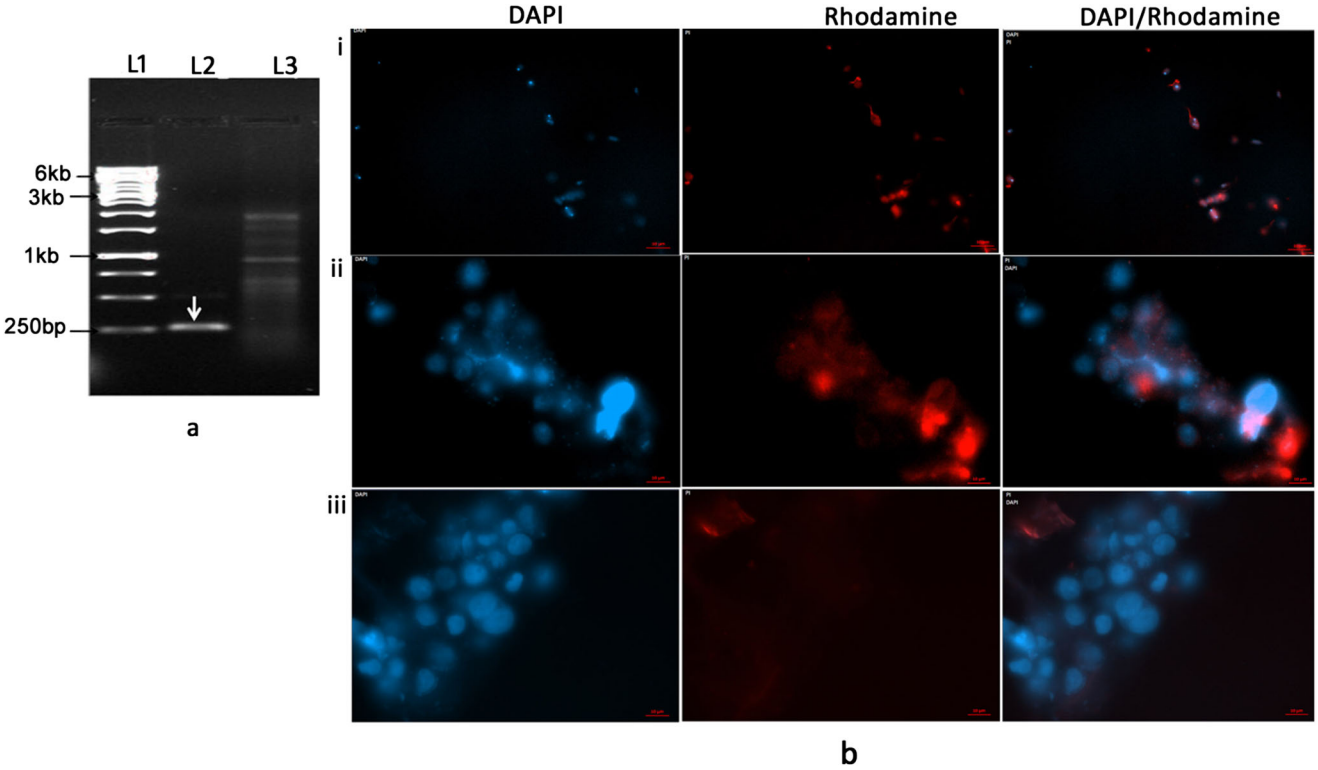

Fig. 3 Stage-specific expression of the native protein in the promastigotes and amastigotes of *L. donovani*. **a** Checking the presence of the partial transcript through reverse transcription PCR with the AMA1 primers and whole-cell RNA isolated from both the promastigotes and amastigotes of *L. donovani*. In respect to the 1-kb DNA ladder in lane 1, the RT-PCR reaction mix with promastigote RNA has produced a sharp band near 250 bp in lane 2 while that of the amastigotes failed to give any in lane 3. **b** Fluorescence microscopy with the promastigotes and the infected THP1 cells carrying the amastigotes of *L. donovani* after probing the native protein with third bleed antiserum and anti-rabbit rhodamine secondary antibody. The filters were used for visualization (461 nm [DAPI] and 636 nm [rhodamine]) and phase contrast microscopy

identified serum albumin to have the maximum identity while conserved domain search led us to derive three domains of albumin superfamily, present in the native protein. Multiple sequence alignment produced > 70% identity with serum albumin bound to myristate and palmitate.

Two 3D models of the pulled-down native protein were generated using the homology modeling procedures with its derived amino acid sequence. The templates with > 70% alignment (Fig. S6) included 1bj5.1.A and 4bke.1.A which are myristate-bound serum albumin and recombinant human serum albumin complexed with palmitate. The SWISS modeler used 1bj5.1.A as a template with a sequence identity of 75.64% for the model MYR, and 4bke.1.A played a role as a template for the PLM model with a sequence identity of 76.61%. The predicted models with bound 2× PLM and 2× MYR produced a Q_{mean} score of − 0.36 (Fig. 5a (i and iii)) and − 1.38 (Fig. 5b (i and iii)), respectively, as per the SWISS modeler system. The models derived from the SWISS modeler also exhibited a local quality estimation quiet above 0.6 for all the two models (Fig. 5a (ii), b (ii)).

Similarly, the MUSTER program was used for 3D structure prediction with the protein threading method after uploading the sequence to the COACH server. It provided a predicted 3D model (Fig. 5c (i) and Fig. S7.1) using the template 1n5uA which is a model derived during the X-ray study of the human serum albumin complexed with heme. The predicted model produced a *z* score of 23.675 with a cutoff value of 6.1. Its local quality estimation was done with PROCHECK (http://services.mbi.ucla.edu/PROCHECK/). Thus, this derived model exhibited least regions with high energy which establishes this model to be quiet stable (Fig. 5c (ii)).

TM-Site (Fig. S7.2), S-Site (Fig. S7.3), COFACTOR (Fig. S7.4), and FINDSITE (Fig. S7.5) results of the COACH server together identified PLM (TM-Site *c* score 0.18) and MYR (TM-Site *c* score 0.51) as probable ligands with other saturated long-chain fatty acids, viz. stearic acid (STE), lauric acid (DAO), capric acid (DKA), and arachidonic acid (ARA) (Fig. S7.1), for the predicted model of the leishmanial native protein.

The models obtained from the SWISS modeler and COACH server were uploaded to Structure Analysis and Verification Server (SAVES) for checking their validity using the compiled tools: ERRAT plot, PROVE, and VERIFY_3D. The PLM and MYR models and the model predicted from the COACH server exhibited 93.12%, 92.43%, and 89.95% of their residues to have an averaged 3D–1D score of ≥ 0.2

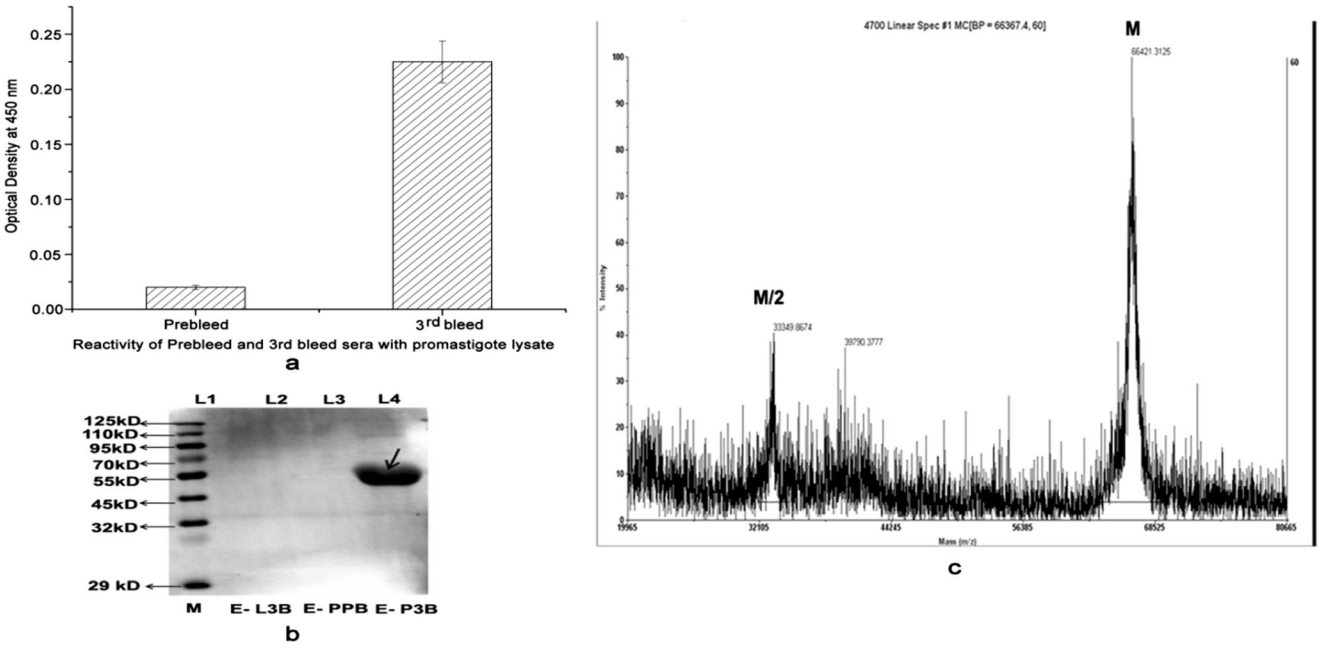

Fig. 4 Level of expression checked in promastigotes and purification of the native protein from the promastigotes with its molecular mass determination through MALDI-TOF MS analysis. **a** Confirmatory ELISA estimation of albumin-like protein in the *L. donovani* promastigote lysate. For detection, the anti-rabbit HRP secondary antibody and TMB-H_2O_2 substrate solution were used with a 450-nm filter. **b** The native protein was purified from the promastigote lysate with the polyclonal IgG molecules of the third bleed serum after cross-linking it with the protein A–Sepharose bead. In respect to a 120–10-kD protein marker at lane 1, the band of the native protein (E-P3B) arrives near the 70-kD marker after probing it with the third bleed serum and anti-rabbit HRP secondary antibody on the PVDF membrane. The negative controls are EL3B and EPPB. In EL3B, the blank lysis buffer was loaded in the bead column of the cross-linked antiserum–protein A (L2). In EPPB, the prebleed serum, devoid of any antibody, was cross-linked with the protein A–Sepharose bead and loaded with promastigote lysate (L3). **c** Determination of the molecular mass of the purified native protein after being singly (M) and doubly (*m*/2) charged with the laser. The *m* peak at 66,421.3 D indicates the molecular mass of the full peptide while the *m*/2 peak at 33,349.9 D refers to the molecular mass of almost half length of the peptide

(Fig. S8) obtained from the VERIFY_3D tool (Job IDs for the PLM-, MYR-, and COACH-predicted models are 269269, 269203, and 269190, respectively) of SAVES (https://services.mbi.ucla.edu/SAVES/), while the ERRAT plot showed the quality factors of 98.594, 93.170, and 93.707, respectively (Fig. S9) for the PLM-predicted (Job ID 92920064), MYR-predicted (Job ID 36391974), and COACH-predicted (Job ID 55594859) models.

The ProSA tool was used for model verification through *z* scores where the comparative protein structure analysis between the model and their corresponding templates was calculated through ProSA and the structural errors were found to be minimum as per the computed *z* scores (Fig. S10).

Finally, the proposed models were checked with the Ramachandran plot where the PLM model has two amino acids (Ala584 and Asp586) present in the generously allowed region (Fig. 6a) and the MYR model has one residue in the disallowed region (Glu588) whereas three other residues (Glu323, Asp335, Asp337) fall in the generously allowed region (Fig. 6b).

Since all these three models have *z* scores of − 12.46, − 12.15, and − 11.92 least distant, it denotes the probability of the native protein to be associated with lipid molecules. The localization of the protein, in respect to membrane cholesterol present in both promastigotes and infected mammalian cells, was further invigilated.

Functional characterization of the native protein

The functional characterization of this native protein was done in two steps. Its correlation with both parasitic membrane cholesterol and infected mammalian membrane cholesterol was investigated through a colocalization study with fluorescence-tagged cholesterol and the fluorescent native protein. The role of this albumin-like protein in infection was confirmed through the antibody-mediated blocking of the native protein molecules present in the outer surfaces of the promastigotes, without hampering the promastigote structural integrity.

Association of the leishmanial albumin-like protein with membrane cholesterol

Sterols are an essential membrane component of eukaryotic cells regulating their mobility. In promastigotes, ergosterols are well documented in their membranes instead of cholesterol

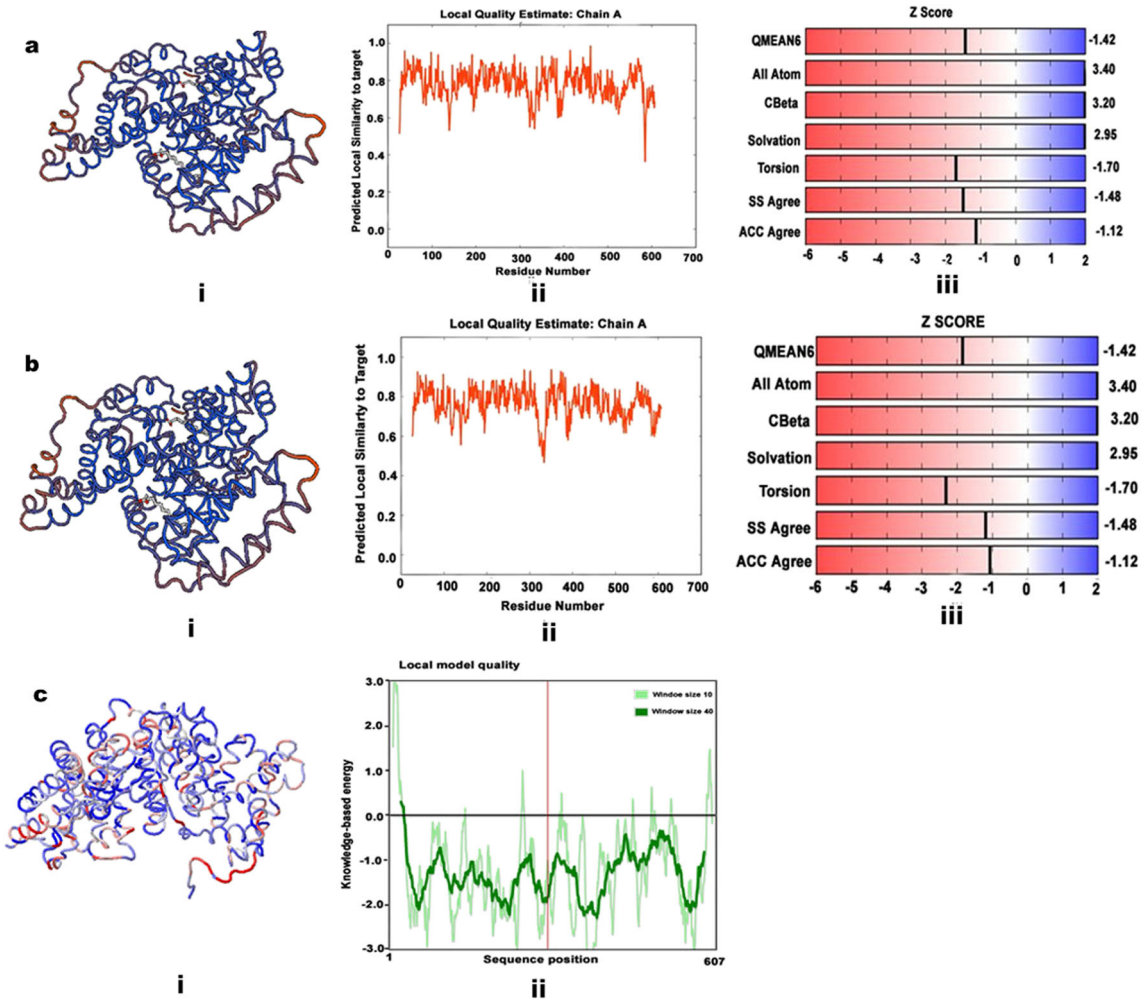

Fig. 5 Three-dimensional structure prediction of the native protein using its amino acid sequence obtained after its LC-MS analysis. **a** Three-dimensional structure (i) predicted through homology modeling using human serum albumin complexed with palmitate as its template (PLM). The local quality estimation graph (ii) and Q_{mean} score (iii) obtained from the SWISS-MODEL system in support of the predicted model. **b** Three-dimensional structure (i) predicted by homology modeling using human serum albumin with bound myristate as its template (MYR). The local quality estimation graph (ii) and Q_{mean} score (iii) obtained from the SWISS-MODEL system in support of the predicted model. **c** Three-dimensional structure (i) predicted by the protein threading method in the COACH server using both palmitate and myristate as putative ligands, supported by its local quality estimation graph (ii)

but the uniqueness is that trypanosomatids lack the cholesterol biosynthetic machinery. Hence, the parasites take up cholesterol from their environment. In this experiment, the promastigotes were cholesterol depleted using methyl-β-cyclodextrin (MBCD) at a concentration of 20 mM which inhibits the uptake of cholesterol through high-density lipoproteins (HDLs) and then the FCS-free media were supplemented with 5 μM NBD-labeled cholesterol which was uptaken by the cholesterol-depleted parasites. Now, the parasites supplemented with NBD-labeled cholesterol were used for fluorescence microscopic analysis after probing the albumin-like protein with the prebleed (Fig. 7a) and third bleed (Fig. 7b) sera. Fluorescence microscopic analysis with prebleed sera which is devoid of any antibody gives no red fluorescence at all (Fig. 7b) while clear colocalization (Fig. 7c, d) of NBD-labeled cholesterol (green) and the leishmanial albumin-like protein (red) is evident in the promastigotes. This colocalization indicates either a mere proximity or an interaction between albumin-like protein and cholesterol in the promastigotes.

Similarly, the infected and uninfected THP1 cells were stained with NBD-labeled cholesterol after cholesterol depletion and the cells were immune probed with the prebleed and third bleed sera raised against the leishmanial partial protein. The infected THP1 control group, stained with the prebleed sera, produced no red fluorescence at all, although they have profound infection (Fig. 7e), while the infected cells probed with the third bleed serum produced to carry the leishmanial native protein in them, clearly colocalized with their membrane cholesterol (Fig. 7f–h). In the uninfected THP1 cells, the cholesterol was stained clearly; however, no trace of fluorescence was evident (Fig. S11) after immune probing with either prebleed or third bleed serum.

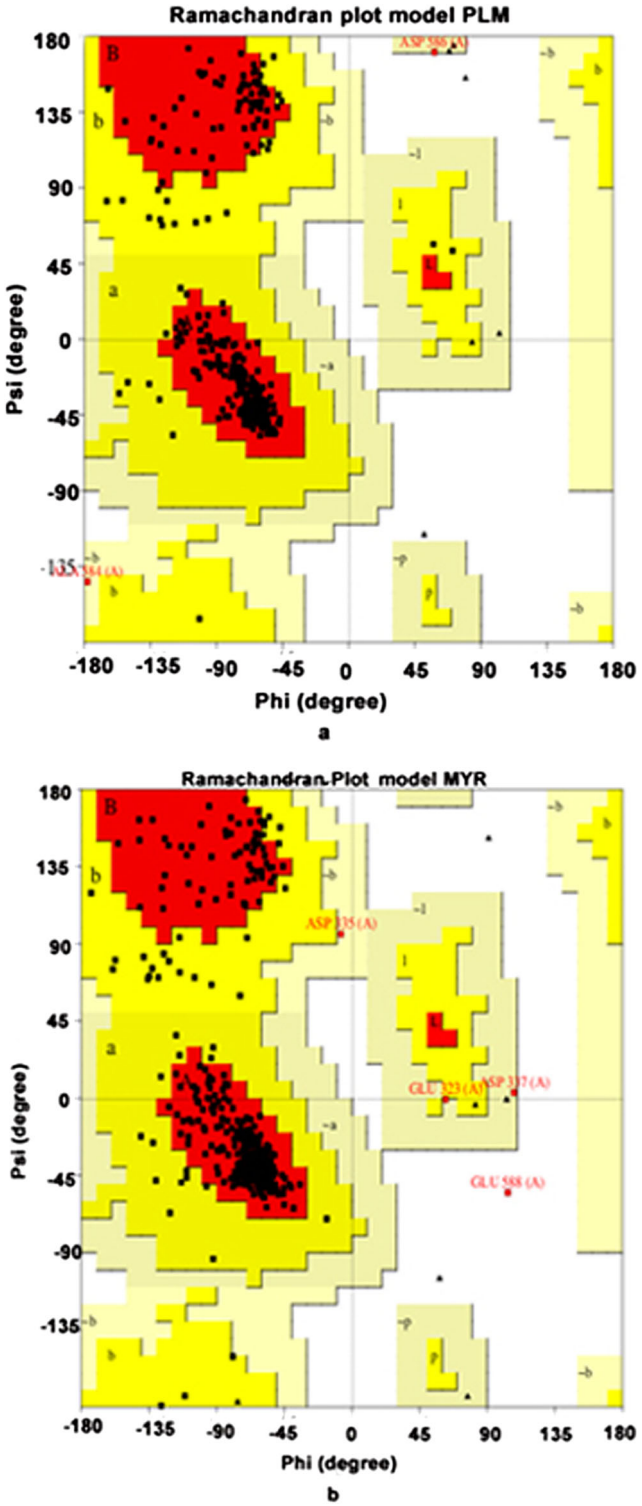

Fig. 6 Validation of the ligand-bound 3D models predicted through homology modeling with the Ramachandran plot. **a** The model predicted to bind to palmitate gives 94.6% of residues to be in the allowed regions with 5% and 0.4% residues in the additional and generously allowed regions, respectively. **b** The model predicted to bind to myristate gives 92.7% of residues to be in the allowed regions with 6.5%, 0.6%, and 0.2% residues in the additional, generously allowed and disallowed regions, respectively

Role of the leishmanial albumin-like protein in parasitic infection

The immune electron microscopy pictures clearly denote the abundance of the leishmanial albumin-like protein molecules on the outer surface of the promastigote membrane. Hence, instead of any genetic or structural disruption, albumin-like surface protein molecules were blocked, simply incubating with its specific antibody. The promastigotes were incubated in the presence and absence of third bleed serum which blocked the albumin-like surface protein and were further checked for their infectivity in the peripheral blood monocytic cells (Fig. 8a). After Giemsa staining of the infected PBMCs, observation under a brightfield microscope (× 100 with oil immersion) revealed the presence of intracellular amastigotes in the PBMCs, infected with the unblocked promastigotes (Fig. 8b). But, the infectivity of the promastigotes was found to be compromised after the antibody-mediated blocking of the albumin-like surface proteins (Fig. 8c) when observed after 24 h. This observation indicates the role of this albumin-like leishmanial surface protein in its infection process, where it may act as a virulence factor similar to the other secretory and membrane-associated factors in parasitism. The gradual increase of infectivity, observed in the T-Inf group, may be due to dilution of the blocking antibody molecules or due to growth medium modification caused by the parasitic metabolite accumulation. The time kinetic analysis of this result is further confirmed by the observations mentioned in Table 2.

Discussion

This article hereby reports a protein, partially encoded by a species-specific stretch of the gene in *Leishmania donovani*. The antiserum produced against the partial peptide identified a leishmanial native protein which is present in the promastigotes as well as in the *L. donovani*-infected THP1 cells. The promastigotes are also evident to express the transcripts while the isolated amastigotes failed to give any. This indicates the expression of this protein to be confined only in the promastigotes. The subcellular localization of this native protein in the *L. donovani* promastigotes was traced by immune electron microscopy, where the comparative subcellular distribution analysis depicts its presence to be highest in the flagella and flagellar pocket and at the outer surfaces of the promastigotes, while nuclei and vesicles are the other sites where a considerable amount of the same protein was also traced. Since in *Trypanosomatids* the flagella and the flagellar pockets are the two main vestibules for secretion and uptake (Landfear and Ignatushchenko 2001) and the electron microscopic images have located the native protein on the outer surfaces of the *L. donovani* promastigotes, it can be postulated

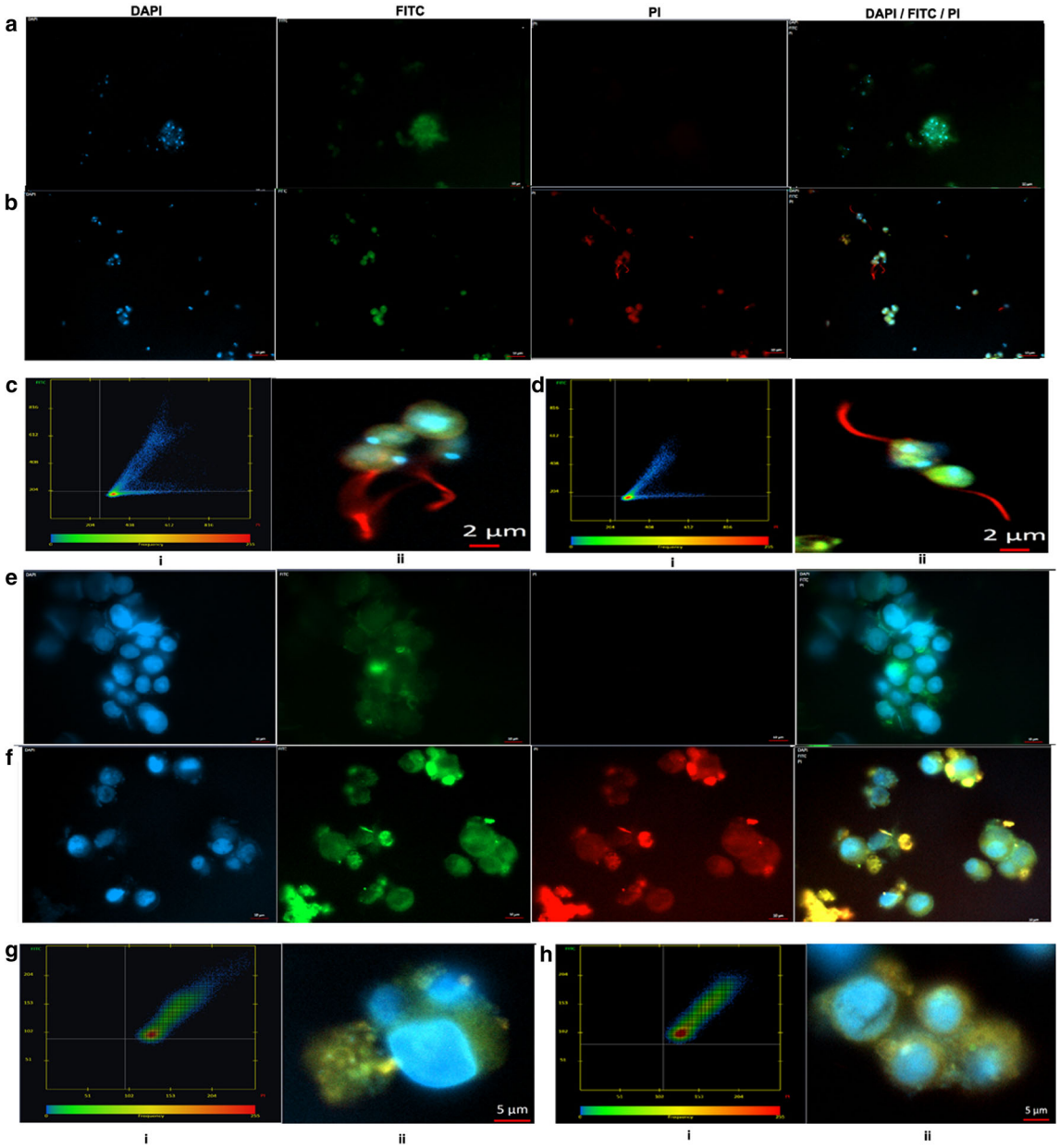

Fig. 7 Association of the leishmanial native protein with the membrane cholesterol in both promastigotes and infected THP1 cells. Colocalization of fluorescently tagged cholesterol (green) and rhodamine-probed native protein (red) was checked through fluorescence microscopy. **a** Microscopic view of *L. donovani* promastigotes labeled with NBD-labeled cholesterol, bearing the native proteins probed with the prebleed serum and rhodamine (negative control). **b** *L. donovani* promastigotes labeled with NBD-labeled cholesterol, bearing the native proteins probed with the third bleed serum and rhodamine. **c**, **d** Scattergram of the green and red fluorescences coming from a single promastigote of *L. donovani* after a × 5 zoom. **e** Microscopic view of the infected THP1 cells labeled with NBD-labeled cholesterol× carrying the native proteins probed with the prebleed serum and rhodamine (negative control). **f** Microscopic view of the infected THP1 cells labeled with NBD-labeled cholesterol× carrying the native proteins probed with the third bleed serum and rhodamine. **g**× **h** Scattergram of the green and red fluorescences coming from the infected cell THP1 cells after a × 2 zoom

that the native protein may have its way out through the flagella and flagellar pocket to the outer surfaces of promastigote.

Further characterization of this native protein required its purification from the whole-cell lysate of promastigotes. The native protein was found to be expressed in adequate level in promastigotes through indirect ELISA assay which took us to follow the oriented affinity method for immunoprecipitation and purification. The protein A–Sepharose bead (Invitrogen 101041) was cross-linked with the polyclonal antibody molecules present in the third bleed serum raised against the leishmanial partial peptide. When promastigote lysate was loaded in this protein A–antibody bead column, it resisted the antibody co-elution and identified a peptide with a molecular

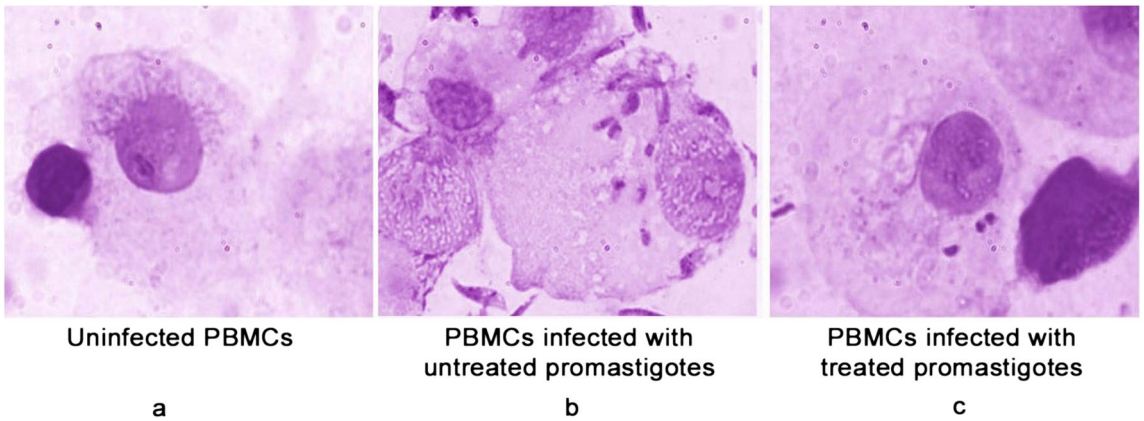

Fig. 8 Elucidation of the role of the native protein in leishmanial infection of isolated PBMCs 24 h after blocking the surface molecules with the third bleed antiserum. **a** Brightfield microscopic analysis (oil immersion) of isolated human PBMCs without any infection. **b** Isolated PBMCs after getting infected with the promastigotes carrying the unblocked protein molecules. **c** Isolated PBMCs after getting infected with the promastigotes having the native protein blocked with the third bleed antiserum

mass of 66.4 kD after MALDI-TOF MS analysis. LC-MS analysis of this peptide band after tryptic digestion detected an amino acid sequence highly similar to serum albumin with three conserved domains of albumin superfamily. As the blocking step with BSA prior to antibody conjugation was not performed, this ruled out the chances of albumin contamination in the eluted sample.

The strongly supportive 3D models of this native protein predicted through homology modeling, viz. MYR and PLM, identified its capability to associate with the long-chain fatty acids, myristate and palmitate, respectively, whereas the 3D model predicted through the protein threading method identified these two and other long-chain fatty acids (stearic acid, lauric acid, capric acid, etc.) as its probable ligands. Model validations through the VERIFY_3D, quality factor of ERRAT2, PROVE, and *z* scores proved all the three models as a probable one while the long-chain fatty acids were the predicted ligands in both the protein threading and homology modeling methods.

A recent study has indicated significant fluctuations in the levels of palmitate and myristate in the promastigotes and amastigotes of *L. donovani* (Bouazizi-Ben Messaoud et al. 2017). The amastigotes have been proved to carry a significantly higher level of palmitate and myristate in respect to the promastigotes, which either may get synthesized immediately after the infection or any specific carrier protein may play a significant role in importing such a huge amount of specific fatty acids. The presence of this native protein in the infected THP1 cells can be an instrumental association of this target protein correlated with the fact that membrane cholesterol may play a role in the trafficking of the membrane lipids.

Finally, the role of this native protein was investigated in the infection procedure through blocking the promastigotes with the albumin-like protein-specific polyclonal antibody. The blocked promastigotes exhibited reduced infectivity towards the host PBMCs. Thus, without any genetic alteration of the promastigotes and the host cells, the invasion was compromised, deciphering the role of this albumin-like protein in infection.

Table 2 Time kinetic study of the percent infectivity of *L. donovani* promastigotes blocked with the crude target antibody. Human PBMCs were exposed to *L. donovani* promastigotes, preincubated with the crude third bleed antiserum (raised against the target albumin-like protein) in a 1:5 ratio up to 72 h. The infection rate is expressed per 100 nuclei of host cell

	INF (per100 nuclei)		T-INF (per 100 nuclei)	
24 h	23	± 0.8	5	± 0.5
48 h	67	± 0.7	12	± 0.62
72 h	130	± 2.1	46	± 0.5

The data was compared with the unblocked promastigote-infected group

Conclusions

From the above study, it may be hypothesized that an albumin-like protein (66.4 kD) is expressed in the extracellular promastigote forms of *L. donovani*, which is capable of binding with long-chain fatty acids, like palmitate and myristate. This albumin-like protein resides mainly in the flagella and flagellar pocket and on the outer surface membrane of the promastigotes being colocalized with the membrane cholesterol molecules. Finally, this albumin-like protein plays an important role in infection which gets compromised if it is blocked by specific antibody. Thus, this protein may be explored as a virulence factor transporting long-chain fatty acids, viz. palmitate and myristate, from the host cells to the intracellular amastigote form for successful parasitism.

Acknowledgements We do hereby acknowledge DST-INSPIRE and UGC, Government of India, for the fellowships provided to the

researchers. We are extremely thankful to Dr. Santu Bandopadhyay and Dr. Nahid Ali, Scientists, CSIR-IICB Kolkata, for providing us with the THP1 human monocytic cell line and *L. donovani* AG83 strain, respectively. We also acknowledge Dr. Ashish Bhattacharjee, Associate Professor, Department of Biotechnology, NIT Durgapur, for his assistance in the LC-MS analysis. Prof. R. Madhubala, Director, AIRF, School of Life Sciences, Jawaharlal Nehru University, is acknowledged for providing the *L. donovani* AG83 strain and Dr. T. C. Nag, Department of Anatomy, AIIMS, New Delhi, for his valuable suggestions in the context of immune electron microscopy.

Data availability The partial sequence of the protein from *Leishmania donovani* is available at http://www.uniprot.org/uniprot/E9BLP2. The partial gene sequence and position can be obtained from https://www.ebi.ac.uk/ena/data/view/CBZ36170 or https://www.ebi.ac.uk/ena/data/view/FR799617 and http://www.genedb.org/gene/LdBPK_301490.1.1:pep, respectively. DNA and protein sequences of the partial protein are available at various databases: EMBL, GenBank, and DDBJ through the FR799617 Genomic DNA and Translation: CBZ36170.1.

Compliance with ethical standards

An institutional ethical committee for human research approval has been taken for the conducted study.

References

Arnold K, Bordoli L, Kopp J, Schwede T (2006) The SWISS-MODEL workspace: a web-based environment for protein structure homology modelling. Bioinformatics 22:195–201. https://doi.org/10.1093/bioinformatics/bti770

Atayde VD, Hassani K, da Silva Lira Filho A et al (2016) Leishmania exosomes and other virulence factors: impact on innate immune response and macrophage functions. Cell Immunol 309:7–18. https://doi.org/10.1016/j.cellimm.2016.07.013

Beck H-P (2002) Extraction and purification of Plasmodium parasite DNA. Methods Mol Med 72:159–163. https://doi.org/10.1385/1-59259-271-6:159

Biasini M, Bienert S, Waterhouse A, Arnold K, Studer G, Schmidt T, Kiefer F, Cassarino TG, Bertoni M, Bordoli L, Schwede T (2014) SWISS-MODEL: modelling protein tertiary and quaternary structure using evolutionary information. Nucleic Acids Res 42:W252–W258. https://doi.org/10.1093/nar/gku340

Bouazizi-Ben Messaoud H, Guichard M, Lawton P, Delton I, Azzouz-Maache S (2017) Changes in lipid and fatty acid composition during intramacrophagic transformation of Leishmania donovani complex promastigotes into amastigotes. Lipids 52:433–441. https://doi.org/10.1007/s11745-017-4233-6

Bowie JU, Lüthy R, Eisenberg D (1991) A method to identify protein sequences that fold into a known three-dimensional structure. Science 253:164–170

Brasselet S, Ferrand P, Kress A (2013) Imaging molecular order in cell membranes by polarization-resolved fluorescence microscopy. Springer Ser Fluoresc 13:311–337. https://doi.org/10.1007/4243

Buffer L, Buffer E, Buffer D (2013) Roberts_purification-of-his-tagged-proteins, pp 3–6

Colovos C, Yeates TO (1993) Verification of protein structures: patterns of nonbonded atomic interactions. Protein Sci 2:1511–1519. https://doi.org/10.1002/pro.5560020916

Couvreur B, Bollen A, Le Ray D, Dujardin J-C (2003) Reverse transcription-polymerase chain reaction construction of plasmid-based, full-length cDNA libraries from Leishmania infantum for in vitro expression screening. Mem Inst Oswaldo Cruz 98:477–480. https://doi.org/10.1590/S0074-02762003000400008

Cox KL, Devanarayan V, Kriauciunas A et al (2004) Immunoassay methods. Eli Lilly & Company and the National Center for Advancing Translational Sciences

Das A, Dasgupta A, Sharma S, Ghosh M, Sengupta T, Bandopadhyay S, Majumder HK (2001) Characterisation of the gene encoding type II DNA topoisomerase from Leishmania donovani: a key molecular target in antileishmanial therapy. Nucleic Acids Res 29:1844–1851

De Castro Levatti EV, Toledo MS, Watanabe Costa R et al (2017) Leishmania (Viannia) braziliensis inositol phosphorylceramide: distinctive sphingoid base composition. Front Microbiol 8:1453. https://doi.org/10.3389/fmicb.2017.01453

Escalona-Montaño AR, Pérez-Montfort R, Cabrera N, Mondragón-Flores R, Vélez-Ramírez DE, Gómez-Sandoval JN, Gutiérrez-Kobeh L, Becker I, Aguirre-García MM (2017) Protein phosphatase PP2C in the flagellum of Leishmania major: cloning and characterization. Parasitol Open 3:e15. https://doi.org/10.1017/pao.2017.14

Farrell JP (2002) Leishmania. Kluwer Academic

Fernandes ACS, Soares DC, Saraiva EM, Meyer-Fernandes JR, Souto-Padrón T (2013) Different secreted phosphatase activities in Leishmania amazonensis. FEMS Microbiol Lett 340:117–128. https://doi.org/10.1111/1574-6968.12080

Furey W, Cowtan KD, Zhang KYJ et al (2006) Programs and program systems in wide use. In: International tables for crystallography. International Union of Crystallography, Chester, pp 695–743

Guex N, Peitsch MC, Schwede T (2009) Automated comparative protein structure modeling with SWISS-MODEL and Swiss-PdbViewer: a historical perspective. Electrophoresis 30:S162–S173. https://doi.org/10.1002/elps.200900140

Gupta G, Oghumu S, Satoskar AR (2013) Mechanisms of immune evasion in leishmaniasis. Adv Appl Microbiol 82:155–184. https://doi.org/10.1016/B978-0-12-407679-2.00005-3

Gupta R, Kumar V, Kushawaha PK, Tripathi CP, Joshi S, Sahasrabuddhe AA, Mitra K, Sundar S, Siddiqi MI, Dube A (2014) Characterization of glycolytic enzymes—rAldolase and rEnolase of Leishmania donovani, identified as Th1 stimulatory proteins, for their immunogenicity and immunoprophylactic efficacies against experimental visceral leishmaniasis. PLoS One 9:e86073. https://doi.org/10.1371/journal.pone.0086073

Hsu F-F, Turk J, Zhang K, Beverley SM (2007) Characterization of inositol phosphorylceramides from Leishmania major by tandem mass spectrometry with electrospray ionization. J Am Soc Mass Spectrom 18:1591–1604. https://doi.org/10.1016/j.jasms.2007.05.017

Kiefer F, Arnold K, Kunzli M, Bordoli L, Schwede T (2009) The SWISS-MODEL repository and associated resources. Nucleic Acids Res 37:D387–D392. https://doi.org/10.1093/nar/gkn750

Kima PE (2016) PI3K signaling in Leishmania infections. Cell Immunol 309:19–22. https://doi.org/10.1016/j.cellimm.2016.09.004

Kowal R, Parsons RG (1980) Stabilization of proteins immobilized on Sepharose from leakage by glutaraldehyde crosslinking. Anal Biochem 102:72–76. https://doi.org/10.1016/0003-2697(80)90319-X

Landfear SM, Ignatushchenko M (2001) The flagellum and flagellar pocket of trypanosomatids. Mol Biochem Parasitol 115:1–17

Laskowski RA, MacArthur MW, Moss DS et al (1993) PROCHECK: a program to check the stereochemical quality of protein structures. J Appl Crystallogr 26:283–291. https://doi.org/10.1107/S0021889892009944

Li W, Cowley A, Uludag M, Gur T, McWilliam H, Squizzato S, Park YM, Buso N, Lopez R (2015) The EMBL-EBI bioinformatics web and programmatic tools framework. Nucleic Acids Res 43:W580–W584. https://doi.org/10.1093/nar/gkv279

Lodge R, Diallo TO, Descoteaux A (2006) Leishmania donovani lipophosphoglycan blocks NADPH oxidase assembly at the phagosome membrane. Cell Microbiol 8:1922–1931. https://doi.org/10.1111/j.1462-5822.2006.00758.x

Lúcia M, Moreno V, De M et al (1998) In vitro method for isolation of amastigote forms of Leishmania amazonensis from J774G8 macrophage induced by temperature shifting. Mem Inst Oswaldo Cruz 93:99–102. https://doi.org/10.1590/S0074-02761998000100017

Lüthy R, Bowie JU, Eisenberg D (1992) Assessment of protein models with three-dimensional profiles. Nature 356:83–85. https://doi.org/10.1038/356083a0

Marchler-Bauer A, Bo Y, Han L, He J, Lanczycki CJ, Lu S, Chitsaz F, Derbyshire MK, Geer RC, Gonzales NR, Gwadz M, Hurwitz DI, Lu F, Marchler GH, Song JS, Thanki N, Wang Z, Yamashita RA, Zhang D, Zheng C, Geer LY, Bryant SH (2017) CDD/SPARCLE: functional classification of proteins via subfamily domain architectures. Nucleic Acids Res 45:D200–D203. https://doi.org/10.1093/nar/gkw1129

McCall L-I, Zhang W-W, Matlashewski G et al (2013) Determinants for the development of visceral leishmaniasis disease. PLoS Pathog 9:e1003053. https://doi.org/10.1371/journal.ppat.1003053

McWilliam H, Li W, Uludag M, Squizzato S, Park YM, Buso N, Cowley AP, Lopez R (2013) Analysis tool web services from the EMBL-EBI. Nucleic Acids Res 41:W597–W600. https://doi.org/10.1093/nar/gkt376

Mina JG, Mosely JA, Ali HZ, Denny PW, Steel PG (2011) Exploring Leishmania major inositol phosphorylceramide synthase (LmjIPCS): insights into the ceramide binding domain. Org Biomol Chem 9:1823–1830. https://doi.org/10.1039/c0ob00871k

Morris AL, MacArthur MW, Hutchinson EG, Thornton JM (1992) Stereochemical quality of protein structure coordinates. Proteins Struct Funct Genet 12:345–364. https://doi.org/10.1002/prot.340120407

Nandan D, Yi T, Lopez M, Lai C, Reiner NE (2002) Leishmania EF-1α activates the Src homology 2 domain containing tyrosine phosphatase SHP-1 leading to macrophage deactivation. J Biol Chem 277:50190–50197. https://doi.org/10.1074/jbc.M209210200

Pillai AB, Xu W, Zhang O, Zhang K (2012) Sphingolipid degradation in Leishmania (Leishmania) amazonensis. PLoS Negl Trop Dis 6:e1944. https://doi.org/10.1371/journal.pntd.0001944

Piscopo TV, Mallia Azzopardi C (2007) Leishmaniasis. Postgrad Med J 83:649–657. https://doi.org/10.1136/PGMJ.2006.047340CORR1

Pontius J, Richelle J, Wodak SJ (1996) Deviations from standard atomic volumes as a quality measure for protein crystal structures. J Mol Biol 264:121–136. https://doi.org/10.1006/jmbi.1996.0628

Raghwan, Chowdhury R (2014) Host cell contact induces fur-dependent expression of virulence factors CagA and VacA in *Helicobacter pylori*. Helicobacter 19:17–25. https://doi.org/10.1111/hel.12087

Rice P, Longden I, Bleasby A (2000) EMBOSS: the European Molecular Biology Open Software Suite. Trends Genet 16:276–277. https://doi.org/10.1016/S0168-9525(00)02024-2

Roychoudhury J, Ali N (2008) Sodium stibogluconate: therapeutic use in the management of leishmaniasis. Indian J Biochem Biophys 45:16–22

Ruhland A, Leal N, Kima PE (2007) Leishmania promastigotes activate PI3K/Akt signalling to confer host cell resistance to apoptosis. Cell Microbiol 9:84–96. https://doi.org/10.1111/j.1462-5822.2006.00769.x

Sengodan SK, Gokulasuriyan RK, Ghosh M (2014) Comparative in-silico genome analysis of Leishmania (Leishmania) donovani: a step towards its species specificity. MGENE 2:782–798. https://doi.org/10.1016/j.mgene.2014.10.003

Shio MT, Hassani K, Isnard A, Ralph B, Contreras I, Gomez MA, Abu-Dayyeh I, Olivier M (2012) Host cell signalling and *Leishmania* mechanisms of evasion. J Trop Med 2012:1–14. https://doi.org/10.1155/2012/819512

Soares-Silva M, Diniz FF, Gomes GN, Bahia D (2016) The mitogen-activated protein kinase (MAPK) pathway: role in immune evasion by trypanosomatids. Front Microbiol 7. https://doi.org/10.3389/FMICB.2016.00183

Soulat D, Bogdan C (2017) Function of macrophage and parasite phosphatases in leishmaniasis. Front Immunol 8:1838. https://doi.org/10.3389/fimmu.2017.01838

Spriestersbach A, Kubicek J, Schäfer F, et al (2015) Purification of his-tagged proteins. In: Methods in enzymology. pp 1–15

Sunter J, Gull K (2017) Shape, form, function and Leishmania pathogenicity: from textbook descriptions to biological understanding. Open Biol 7. https://doi.org/10.1098/rsob.170165

Verma AK, Laha B, Pandey M, Pal U, Ghosh M (2017) Cholesterol-lowering drug, in combination with chromium chloride, induces early apoptotic signals in intracellular L. donovani amastigotes, leading to death. J Biosci 42:427–438. https://doi.org/10.1007/s12038-017-9690-9

Wiederstein M, Sippl MJ (2007) ProSA-web: interactive web service for the recognition of errors in three-dimensional structures of proteins. Nucleic Acids Res 35:W407–W410. https://doi.org/10.1093/nar/gkm290

Yang J, Roy A, Zhang Y (2013a) BioLiP: a semi-manually curated database for biologically relevant ligand-protein interactions. Nucleic Acids Res 41:1096–1103. https://doi.org/10.1093/nar/gks966

Yang J, Roy A, Zhang Y (2013b) Protein-ligand binding site recognition using complementary binding-specific substructure comparison and sequence profile alignment. Bioinformatics 29:2588–2595. https://doi.org/10.1093/bioinformatics/btt447

Zhang K, Beverley SM (2010) Phospholipid and sphingolipid metabolism in Leishmania. Mol Biochem Parasitol 170:55–64. https://doi.org/10.1016/j.molbiopara.2009.12.004